International Journal of Non-Linear Mechanics 44 (2009) 257 – 262

Contents lists available at ScienceDirect

International Journal of Non-Linear Mechanics

journal homepage: www.elsevier.com/locate/nlm

Analytical and numerical solutions for shapes of quiescent two-dimensional vesicles

Shravan K. Veerapaneni[a], Ritwik Raj[b], George Biros[b,c,d], Prashant K. Purohit[b,*]

[a]Courant Institute of Mathematical Sciences, New York University, NY 10012, USA
[b]Department of Mechanical Engineering and Applied Mechanics, University of Pennsylvania, Philadelphia, PA 19104, USA
[c]Department of Bioengineering, University of Pennsylvania, Philadelphia, PA 19104, USA
[d]Department of Computer and Information Science, University of Pennsylvania, Philadelphia, PA 19104, USA

ARTICLE INFO

Article history:
Received 2 April 2008
Received in revised form 17 October 2008
Accepted 22 October 2008

Keywords:
Vesicles
Helfrich energy

ABSTRACT

We describe an analytic method for the computation of equilibrium shapes for two-dimensional vesicles characterized by a Helfrich elastic energy. We derive boundary value problems and solve them analytically in terms of elliptic functions and elliptic integrals. We derive solutions by prescribing length and area, or displacements and angle boundary conditions. The solutions are compared to solutions obtained by a boundary integral equation-based numerical scheme. Our method enables the identification of different configurations of deformable vesicles and accurate calculation of their shape, bending moments, tension, and the pressure jump across the vesicle membrane. Furthermore, we perform numerical experiments that indicate that all these configurations are stable minima.

1. Introduction

The evolution of vesicle dynamics is characterized by a competition between membrane elastic energy, inextensibility, and the nonlocal hydrodynamic forces [1]. Inextensible vesicles have received a lot of attention as they are present in many biological phenomena [2] and have been used to understand properties of biological membranes [3]. Experiments on vesicle tumbling, tank-treading, and deformation under shear flow have been conducted by various groups [4–8]. In addition, vesicles have been used as models for red blood cells [9,10] and drug-carrying capsules [11].

The observable of interest in both equilibrium and dynamic studies of vesicles is their shape, but few analytical solutions exist for calculating the shape under various constraints. The known closed form solutions solve the shape equation for axisymmetric vesicles for special boundary conditions [12]. The shape equation for axisymmetric vesicles is a fourth order non-linear ordinary differential equation and a general solution to this equation has not been obtained. The analogue of the shape equation in two dimensions is more amenable to analysis and provides valuable insight for the axisymmetric problem, and has been treated by many authors [13–15]. For example, Arreaga et al. [13]give a detailed analysis of elastic loops under area and length constraints and obtain analytic solutions for the shape, assuming known tension and pressure. Shi et al. [14] consider adhesion of two-dimensional vesicles on curved substrates and obtain force deformation relationships for the vesicle as a function of substrate shape. The analysis of Shi et al. follows the work of Seifert [15] who obtained shape equations for two-dimensional vesicles both in the presence and absence of adhesive forces. Seifert uses a series solution to obtain lowest energy shapes of free vesicles for various values of the prescribed pressure difference and shows that the shapes obtained using the two-dimensional theory are similar to those obtained by numerically solving the axisymmetric shape equations.

Computation of the vesicle shape is also key to interpreting an interesting class of experiments involving interactions of microtubules and lipid vesicles as reported in Fygenson et al. [16]. In this experiment, the authors were able to induce shape changes in vesicles by growing microtubules within them. In order to determine the vesicle shape, the authors minimize a free energy by representing the vesicle contour by lines and circular arcs instead of solving the shape equation for axisymmetric vesicles with the appropriate boundary conditions. Also, they look at the slope of the free energy of the equilibrium shape with respect to different values of the microtubule length and determine the force exerted by the membrane on the microtubule. Solving the axisymmetric shape equation for the constraints imposed by the microtubule, to the best of our knowledge, has not been done before. In this paper, we give a solution of the two-dimensional analogue of this problem to develop intuition for solving the axisymmetric problem.

Contributions: We present an analytical method for the calculation of two-dimensional equilibrium shapes of quiescent vesicles immersed in stationary fluids. *First*, we consider the case in which

* Corresponding author. Tel.: +1 215 898 3870.
E-mail addresses: shravan@cims.nyu.edu (S.K. Veerapaneni), ritwikr@seas.upenn.edu (R. Raj), biros@seas.upenn.edu (G. Biros) (P.K. Purohit).

0020-7462/$ - see front matter © 2008 Published by Elsevier Ltd.
doi:10.1016/j.ijnonlinmec.2008.10.004

we prescribe area and length constraints, and then (1) derive equilibrium shapes analytically, and (2) verify them using a numerical scheme developed in our group [17]. To an extent, our construction is similar to the one presented in [13] but we prescribe different, and perhaps more natural, constraints on the vesicle. In [13], the authors prescribe pressure and tension. We prescribe either area and length constraints or displacements between two parts of vesicles along with angle or curvature information. *Second*, our numerical scheme is capable of tracking the evolution of the shape of a vesicle and the motion of the fluid around it, starting from arbitrary initial conditions. It therefore gives us the path to equilibrium, and is more sophisticated than solving the equilibrium equations alone. The method is described in brief in this paper, and in more detail elsewhere [17]. *Third*, we consider the setting of [16], and obtain similar shapes as the ones reported in their experiment by solving a boundary value problem for the vesicle. In this way, we can explicitly determine the force on the microtubule, but in addition we can also compute the bending moment exerted by the membrane on the microtubule. The bending moment determines how easily the microtubule will develop a curvature (or buckle) as it pushes on the vesicle. Our study complements that of Heinrich et al. [18] who compute the shapes ofaxisymmetric vesicles under an axial load. Heinrich et al. discuss two ensembles—one, in which the axial force is prescribed, and the other, in which the distance between the two poles of the vesicle is prescribed—but give explicit solutions only for the former case. Their solutions are applicable in a situation where optical or magnetic beads are used to exert forces on the vesicle [18], where as, our method is appropriate for cases where a microtubule enforces a distance constraint between two points on the vesicle [16].

2. Problem formulation

In this section, we state the equations that determine the vesicle equilibrium shape. There are two different (but related) ways to derive these equations: the variational approach, which we use to construct analytic solutions, and a fluid-structure dynamics approach, which we use for numerical computations. In the variational approach, the equilibrium shape is solved as a constrained minimization problem: we seek to find the shape that minimizes the bending energy of the membrane assuming we know its length and enclosed area. In the dynamics approach, we model the dynamics of an arbitrary-shaped, locally inextensible vesicle. The interior and exterior of the vesicle are occupied by a stationary incompressible Stokesian fluid. The vesicle induces a velocity field in the fluid due to its membrane forces and due to the no-slip coupling boundary condition at the interface. We solve the governing equation of the fluid numerically, until the velocity field becomes zero. The vesicle shape at the end of the simulation is the equilibrium shape.

Variational approach: We introduce Lagrange multipliers σ (tension) and p (pressure), for the length and area constraints, respectively, and we seek stationary points of the Lagrangian

$$\mathscr{L} = \int_\gamma \frac{\kappa^2}{2}\,\mathrm{d}\gamma + \sigma\left(\int_\gamma \mathrm{d}\gamma - L\right) + p\left(\int_\gamma \frac{1}{2}\mathbf{x}\cdot\mathbf{n}\,\mathrm{d}\gamma - A\right),$$

where κ is the curvature, γ is the boundary of the vesicle, $\mathbf{x}$ is a point on γ, $\mathbf{n}$ is the unit normal, L is the length, and A is the enclosed area. Without loss of generality, we assume a unit bending modulus for the membrane. The force acting on the membrane is computed by taking variations of $\mathscr{L}$ with respect to γ. This force can be written as a sum of a force due to bending $\mathbf{f}_\kappa = (\kappa_{ss} + \kappa^3/2)\mathbf{n}$, a force due to tension $\mathbf{f}_\sigma = -\sigma\kappa\mathbf{n}$, and a force due to pressure $\mathbf{f}_p = p\mathbf{n}$, where s is the arc-length and $\mathbf{t}$ is the tangent at a point on γ. At equilibrium, $\mathbf{f}_\kappa + \mathbf{f}_\sigma + \mathbf{f}_p = 0$. The force balance in the normal direction yields a second-order, inhomogeneous, non-linear differential equation for the curvature κ, which is given by

$$\kappa_{ss} + \tfrac{1}{2}\kappa^3 - \sigma\kappa + p = 0. \tag{1}$$

The constants σ and p are determined from the specified length and area of the vesicle. We impose periodic boundary conditions and solve (1) analytically; given κ, the shape of the vesicle is determined uniquely [19].

Dynamics approach: The surrounding fluid is assumed to be Stokesian with unit viscosity [20]. The total membrane force is the sum of a force due to bending $\mathbf{f}_\kappa$ and due to the inextensibility $\mathbf{f}_\sigma$. The tension (σ) acts as a Lagrange multiplier enforcing the inextensibility *locally*. As a result, the expression for $\mathbf{f}_\sigma$ involves an additional term and is given by $\mathbf{f}_\sigma = \sigma_s\mathbf{t} - \sigma\kappa\mathbf{n}$, where $\mathbf{t}$ is the unit tangent vector. Let $\mathbf{x}$ be the position of the vesicle boundary. The vesicle dynamics is governed by

$$\dot{\mathbf{x}} = \mathscr{S}[\mathbf{f}_\kappa + \mathbf{f}_\sigma](\mathbf{x}) \quad \text{and} \quad \mathbf{t}\cdot\frac{\mathrm{d}}{\mathrm{d}s}\dot{\mathbf{x}} = 0, \tag{2}$$

the momentum and the local inextensibility constraint, respectively. We enforce the local inextensibility by requiring the surface divergence ($\mathbf{t}\cdot\mathrm{d}/\mathrm{d}s$) of the velocity field ($\dot{\mathbf{x}}$) on the fluid–vesicle interface to vanish. The free-space Stokes single-layer potential $\mathscr{S}[\mathbf{f}]$ is defined by $\mathscr{S}[\mathbf{f}](\mathbf{x}) = \int_\gamma G(\mathbf{x}-\mathbf{y})\mathbf{f}(\mathbf{y})\,\mathrm{d}s(\mathbf{y})$ with

$$G(\mathbf{r}) = \frac{1}{4\pi}\left(-\ln\|\mathbf{r}_2\|\,\mathbf{I} + \frac{\mathbf{r}\otimes\mathbf{r}}{\|\mathbf{r}\|_2^2}\right) \quad \text{and} \quad \mathbf{r} = \mathbf{x}-\mathbf{y}. \tag{3}$$

For a locally inextensible vesicle, the force due to curvature can equivalently be written as $\mathbf{f}_\kappa = -\mathbf{x}_{ssss}$ (see [17, Appendix A]). Following the identity $\mathbf{x}_{ss} = -\kappa\mathbf{n}$, the tension force can be written as $\mathbf{f}_\sigma = (\sigma\mathbf{x}_s)_s$. In two-dimensional, the surface divergence of a vector field $\mathbf{v}$ is given by $\mathbf{t}\cdot(\mathrm{d}/\mathrm{d}s)\mathbf{v} = \mathbf{x}_s\cdot\mathbf{v}_s$. Substituting these expressions into Eq. (2), we get

$$\dot{\mathbf{x}} = -\mathscr{S}[\mathbf{x}_{ssss}](\mathbf{x}) + \mathscr{S}[(\sigma\mathbf{x}_s)_s](\mathbf{x}) \quad \text{and}$$
$$\mathbf{x}_s\cdot(\mathscr{S}[(\sigma\mathbf{x}_s)_s])_s = \mathbf{x}_s\cdot(\mathscr{S}[\mathbf{x}_{ssss}])_s. \tag{4}$$

3. Solution methodology

In this section, we construct analytical solutions for (1) and discuss a numerical scheme for solving the fluid-structure dynamics problem (4).

3.1. Analytic solution

From Eq. (1), we integrate over the arc-length s and get

$$\frac{\kappa_s^2}{2} + \frac{\kappa^4}{8} - \frac{\sigma}{2}\kappa^2 + p\kappa = C, \tag{5}$$

where C is a constant. Without loss of generality we assume that $\kappa_s = 0$ at $s = 0$ and $\kappa(0) = \kappa_0$. We then eliminate C and rewrite the differential equation above as

$$\int_y^\infty \frac{\mathrm{d}y}{\sqrt{y^3 + \dfrac{Q}{P}y^2 + \dfrac{\kappa_0}{P}y - \dfrac{1}{4P}}} = \int_s^0 \sqrt{P}\,\mathrm{d}s, \tag{6}$$

where we have introduced a new variable $y(s) = 1/(\kappa_0 - \kappa(s))$ and the constants P and Q are given in terms of the tension σ and pressure p by

$$P = \kappa_0^3 - 2\sigma\kappa_0 + 2p, \tag{7}$$
$$Q = \frac{-3\kappa_0^2}{2} + \sigma. \tag{8}$$

There are three unknown parameters P, Q, and κ_0 in these equations and they will be determined by imposing three constraints as we

shall show later. The integral on the left-hand side of (6) can be calculated in terms of elliptic functions, assuming that the cubic in the radical has only one real root α [21] and admits the factorization:

$$y^3+\frac{Q}{P}y^2+\frac{\kappa_0}{P}y-\frac{1}{4P}=(y-\alpha)[(y-m)^2+n^2], \tag{9}$$

where m and n are real. The result is

$$\int_{y(s)}^{\infty}\frac{\mathrm{d}y}{\sqrt{y^3+\frac{Q}{P}y^2+\frac{\kappa_0}{P}y-\frac{1}{4P}}} =\frac{\sqrt{2}}{\sqrt{y_1-y_3}}\,\mathrm{cn}^{-1}\left(\frac{y(s)-y_1}{y(s)-y_3}\middle|\sqrt{\frac{m-y_3}{y_1-y_3}}\right), \tag{10}$$

where y_1 and y_3 are roots of the quadratic equation

$$y^2-2\alpha y+2m\alpha-(m^2+n^2)=0. \tag{11}$$

It follows from (6) that

$$\kappa(s)=\kappa_0-\frac{1-\mathrm{cn}\left(-\frac{\sqrt{P(y_1-y_3)}s}{\sqrt{2}}\middle|\sqrt{\frac{m-y_3}{y_1-y_3}}\right)}{y_1-y_3\mathrm{cn}\left(-\frac{\sqrt{P(y_1-y_3)}s}{\sqrt{2}}\middle|\sqrt{\frac{m-y_3}{y_1-y_3}}\right)}. \tag{12}$$

Remark. We could have also started with the possibility that the cubic in the radical of (7) has three real roots, but this leads to a contradiction. To see this we assume that $y^3+(Q/P)y^2+(\kappa_0/P)y-1/4P=(y+a)(y+b)(y+c)$, where a, b, c are real and satisfy $a>b>c$. This amounts to assuming that there are four distinct values of κ at which $\kappa_s=0$. The differential equation (7) can now be integrated by methods analogous to those for the imaginary roots and the solution turns out to be $\kappa(s)=\kappa_0-\mathrm{sn}^2(\sqrt{2abc(c-a)}s|\sqrt{(a-b)/(a-c)})/((a-c)-a\mathrm{sn}^2(\sqrt{2abc(c-a)}s|\sqrt{(a-b)/(a-c)}))$. Corresponding to this solution the extrema of $\kappa(s)$ are κ_0-1/c and κ_0 which contradicts our assumption that there are four distinct values at which $\kappa_s=0$. Therefore, (12) is the final solution for the curvature.

The constants κ_0, P and Q can be written in terms of m, y_1 and y_3 as follows:

$$\kappa_0=\frac{2m-\frac{y_1y_3}{y_1+y_3}}{2m(y_1+y_3)-2y_1y_3},\quad P=\frac{(y_1+y_3)\kappa_0-0.5}{m(y_1+y_3)^2},$$
$$Q=-P\left(2m+\frac{y_1+y_3}{2}\right). \tag{13}$$

We impose the following constraints on the solution to determine κ_0, P and Q (or equivalently m, y_1 and y_3).

1. *Periodicity of* κ: A closed vesicle of length L satisfies the periodicity condition $\mathbf{x}(0)=\mathbf{x}(L)$, where $\mathbf{x}(s)=[x_1(s)\ x_2(s)]$. This and the smoothness of $\mathbf{x}(s)$ imply that the curvature $\kappa(s)$ is periodic and satisfies $\kappa(L)=\kappa(0)=\kappa_0$. In order to enforce this constraint, we first observe that (12) is already periodic since the elliptic function $\mathrm{cn}(s|k)$ satisfies $\mathrm{cn}(s|k)=\mathrm{cn}(s+4qK(k)|k)$ where $K(k)$ is the complete elliptic integral of the first kind and q is an integer. We enforce $\kappa(L)=\kappa_0$ by requiring that

$$\sqrt{\frac{P(y_1-y_3)}{2}}L=4qK\left(\sqrt{\frac{m-y_3}{y_1-y_3}}\right). \tag{14}$$

Note that the minimum value of q is 2; by the four-vertex theorem for a closed planar curve [22], there exist at least two minima and two maxima in κ. Setting $q=2$ gives two lobed vesicles (see Fig. 1). By choosing $q\geqslant 2$ we obtain q-lobed vesicles. In particular, we have obtained three- and four-lobed shapes.

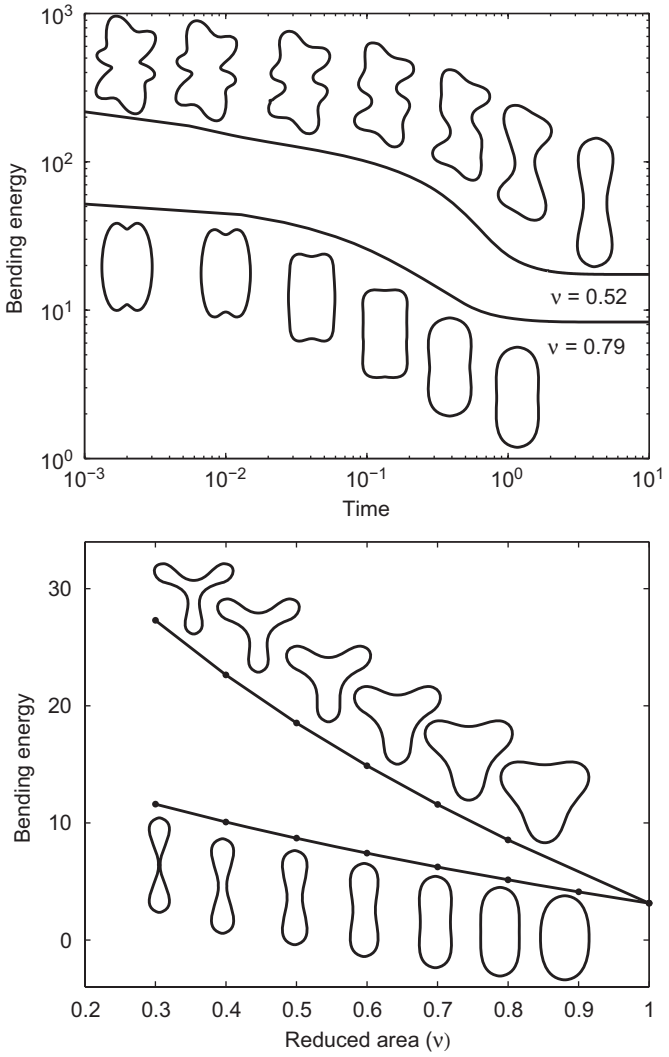

Fig. 1. In the *top figure*, we report the elastic energy as a function of time for two vesicles with different reduced areas v. We also plot the evolution of the vesicle shapes to an equilibrium state. Notice that the smaller the reduced area the higher the bending energy. In the *bottom figure*, we report the bending energy as a function of the reduced area v for two different vesicle configurations both of which are stable local minima. We can characterize the configurations by the number of lobes. Also, we show the equilibrium shapes corresponding to different reduced areas. The bending energy increases with increasing number of lobes and decreasing reduced area. The equilibrium shapes in both the figures coincide with the analytically computed ones to several digits.

2. *Length of the contour is* L: As the angle θ made by the tangent to the x_1-axis goes from 0 to 2π, we traverse a length L along the vesicle contour. Said differently, the tangent to the vesicle contour rotates through 2π rad as we go from $s=0$ to L. Hence we require

$$\int_0^L\kappa(s)\,\mathrm{d}s=\theta(L)-\theta(0)=2\pi. \tag{15}$$

3. *Area enclosed by the contour is* A: The final constraint is imposed on the area enclosed by the contour. We prescribe an area A such that $A\leqslant L^2/4\pi$ and enforce it as follows:

$$\int_0^L x_2\cos\theta\,\mathrm{d}s=A, \tag{16}$$

where we define $x_1(s)=\int_0^s\cos\theta\,\mathrm{d}s$ and $x_2(s)=\int_0^s\sin\theta\,\mathrm{d}s$.

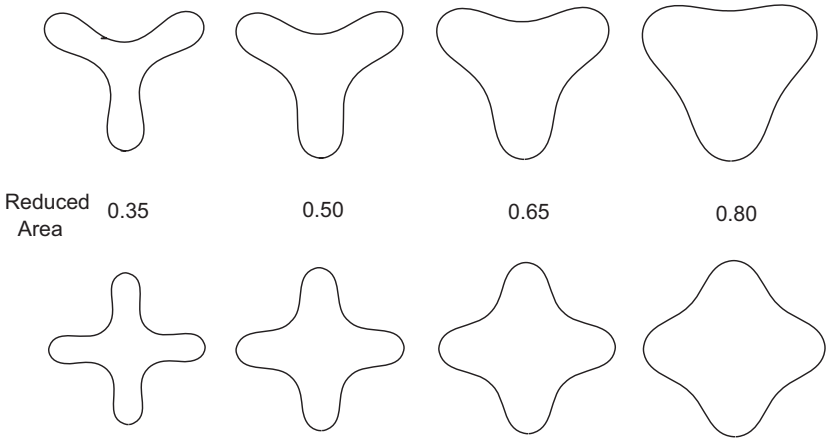

Fig. 2. Three- and four-lobed equilibrium shapes. Each of these shapes wasprescribed as initial condition for the numerical scheme and velocity fields in the surrounding fluid were determined as the vesicle relaxed. The induced velocities were nearly zero showing that these shapes are indeed at equilibrium. When small perturbations were added to the shapes they relaxed back to the same equilibrium, leading us to conclude that these are stable configurations.

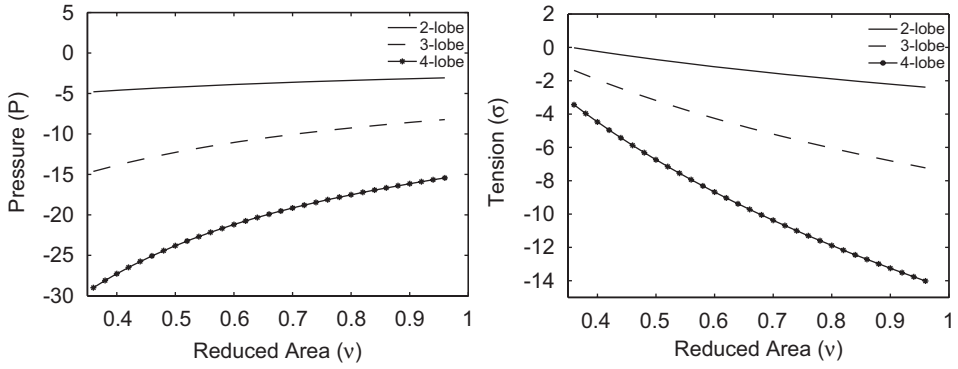

Fig. 3. The tension and pressure difference plotted as a function of the reduced area v for vesicles of length 2π. Note that as $v \to 1$ (which corresponds to a circular vesicle) we approach different values of the pressure and tension depending on the number of lobes in the vesicle. The limiting values of p and σ for the circular vesicle satisfy $1/2R^3 - \sigma R + p = 0$ where R is the radius of vesicle.

These constraints reinforce the known fact that the shape of the vesicle is determined entirely by the reduced area $v = 4\pi A/L^2$ and the number of lobes q. The resulting algebraic equations for P, Q, and κ_0 are solved numerically using Newton's method. For a given reduced area, we start with different values of the initial guess for the root for different values of q. Once, we have obtained convergence for one value of the reduced area, roots for the other values of reduced area can be obtained by continuation. The tension σ and pressure difference p for a given reduced area then follow immediately as solutions of (7) and (8). Shapes of two- and three-lobed vesicles for various values of the reduced area v and their corresponding bending energy are shown in Fig. 1.

3.2. Numerical solution

The presence of high-order spatial derivatives in $\mathbf{f}_\kappa$ makes the evolution equation (4) numerically *stiff* [23]. As a result, numerical solution through a fully explicit time-marching scheme will be computationally expensive. To overcome this issue, a semi-implicit scheme was proposed in [17]. Starting from arbitrary initial shapes, we use this scheme to compute the equilibrium shapes. We briefly discuss this scheme here.

Let $\mathbf{x}(\alpha, t)$ be a point on $\gamma(t)$, where $\alpha \in [0, 2\pi]$ parameterizes the boundary. The numerical scheme is based on discretizing uniformly in space $\{\alpha_k = 2\pi k/M\}_{k=0}^{M-1}$ and time $\{n\Delta t\}_{n=1}^{N}$. A Fourier basis is used to represent the boundary and the derivatives on $\mathbf{x}$ are computed spectrally. Let $\hat{\mathbf{x}}(m, t)$, $m = -M/2, \ldots, M/2 - 1$ be the Fourier coefficients of $\mathbf{x}(\alpha, t)$. We compute $\mathbf{x}_\alpha$ by

$$\mathbf{x}_\alpha(\alpha, t) = \sum_{m=-M/2}^{M/2-1} (-\mathrm{i}m)\hat{\mathbf{x}}(m, t)\mathrm{e}^{-\mathrm{i}m\alpha}. \tag{17}$$

The derivatives with respect to arclength s are computed by $\mathbf{x}_s = \mathbf{x}_\alpha/|\mathbf{x}_\alpha|$, where we substituted $s_\alpha = |\mathbf{x}_\alpha|$. Hereafter, we use $|\mathbf{x}_\alpha|$ to denote the magnitude of $\mathbf{x}_\alpha$, that is, $|\mathbf{x}_\alpha| = \sqrt{x_{1\alpha}^2 + x_{2\alpha}^2}$.

Let $\mathbf{x}^n$ denote the position at $n\Delta t$. Then a first-order time-marching scheme for (4) is given by

$$\begin{aligned}\frac{\mathbf{x}^{n+1} - \mathbf{x}^n}{\Delta t} = &\int_0^{2\pi} G(\mathbf{x}^n, \mathbf{y}^n)\left(\frac{1}{|\mathbf{y}_\alpha^n|}\left(\frac{1}{|\mathbf{y}_\alpha^n|}\left(\frac{\mathbf{y}_\alpha^{n+1}}{|\mathbf{y}_\alpha^n|}\right)_\alpha\right)_\alpha\right)_\alpha \mathrm{d}\alpha \\ &+ \int_0^{2\pi} G(\mathbf{x}^n, \mathbf{y}^n)\left(\sigma^{n+1}\frac{\mathbf{y}_\alpha^n}{|\mathbf{y}_\alpha^n|}\right)_\alpha \mathrm{d}\alpha,\end{aligned} \tag{18}$$

$$\begin{aligned}&\mathbf{x}_\alpha^n \cdot \int_0^{2\pi} G(\mathbf{x}^n, \mathbf{y}^n)\left(\sigma^{n+1}\frac{\mathbf{y}_\alpha^n}{|\mathbf{y}_\alpha^n|}\right)_\alpha \mathrm{d}\alpha \\ &\quad = -\mathbf{x}_\alpha^n \cdot \int_0^{2\pi} G(\mathbf{x}^n, \mathbf{y}^n)\left(\frac{1}{|\mathbf{y}_\alpha^n|}\left(\frac{1}{|\mathbf{y}_\alpha^n|}\left(\frac{\mathbf{y}_\alpha^{n+1}}{|\mathbf{y}_\alpha^n|}\right)_\alpha\right)_\alpha\right)_\alpha \mathrm{d}\alpha.\end{aligned} \tag{19}$$

Table 1
We computed the equilibrium shape of the topmost vesicle shown in Fig. 1 analytically.

M	16	32	64	128
$\|\mathbf{v}(\mathbf{x})\|_\infty$	4.32e − 001	8.40e − 004	7.79e − 009	3.21e − 010

The velocity field (4) evaluated on this shape must be zero. Here, we report the max-norm errors in computing the velocity. M is the number of spatial discretization points on the vesicle used by our numerical scheme. Since our spatial discretization scheme is spectral and the quadrature rules are high-order, the error decays rapidly.

The tension and the term in the bending force with highest order derivatives on the position are treated implicitly. The rest of the terms are treated explicitly. The high-order quadrature rules of [24], designed to handle the logarithmic singularity, are used to compute the integrals. The unknowns are the position $\mathbf{x}^{n+1}$ and tension σ^{n+1} at $\{\alpha_k\}_{k=0}^{M-1}$. The system of coupled equations (18) and (19) is linear in the unknowns and solved using GMRES [25].

4. Results

We compute the equilibrium shapes by using the numerical scheme (18) and (19) with an arbitrary initial shape and by solving the constraint equations (14)–(16) and evaluating (12). In Fig. 1, we plot a sample outcome of these computations. In the top figure, we plot the snapshots of two vesicles relaxing to equilibrium. In the bottom figure, we plot the analytically computed equilibrium shapes for different reduced areas. Further, in Fig. 2, we show the three- and four-lobed equilibrium shapes. The parameters σ and p in Eq. (1) corresponding to different equilibrium configurations are plotted in Fig. 3.

At equilibrium, the tension and bending forces in Eq. (4) balance each other. Hence $\dot{\mathbf{x}}$ should vanish for an equilibrium shape. We use this fact for comparing our numerical and analytical solutions. We supply the analytic solution as an initial condition to the numerical scheme. If the analytical solution is indeed a minimum energy configuration for that particular reduced area, the velocity field ($\dot{\mathbf{x}}$) induced by this shape must be zero. In Table 1, we report the maximum velocity for different spatial discretizations. We observe that as the spatial discretization is refined, the error converges to zero. This convergence illustrates the excellent agreement between our analytical and numerical computations.

Using our numerical scheme, we also verified that the shapes with $q \geqslant 3$ are indeed *stable equilibria*. This is done by slightly perturbing the equilibrium shapes and verifying that they relax to a shape with the same number of lobes. The same conclusion is not true for vesicles in three dimensions as shown by Peterson [15,26]. In two dimensions Arreaga et al. [13] showed that shapes with $q \geqslant 3$ can indeed be obtained as solutions to the equilibrium equations, but they have higher energy than the corresponding two-lobed shapes, which is consistent with our results.

5. Shape of the vesicle in the presence of a microtubule

Prescribing the area enclosed by the vesicle is one way of controlling its shape. The shape can also be controlled by other methods, e.g., by growing microtubules within the vesicle [16]. The tension σ and pressure difference p in this problem are determined again by first solving for the shape. In order to illustrate this procedure, we consider the special case of $p=0$ and solve for the shape of the vesicle under a displacement constraint imposed by the microtubule. The equation of equilibrium now reads

$$\kappa_{ss} + \frac{\kappa^3}{2} - \sigma\kappa = 0. \tag{20}$$

The solution to this equation can be written in terms of elliptic functions as follows:

$$\kappa = \frac{1}{\lambda}\mathrm{dn}\left(\frac{s}{2\lambda}\middle| k\right) \quad \text{and} \quad k^2 = 2 - 4\sigma\lambda^2, \tag{21}$$

where λ is a length scale and k is a constant depending on the tension σ. We integrate this once to obtain $\theta(s) = 2\mathrm{am}(s/2\lambda|k)$, where the integration constant has been eliminated by enforcing $\theta(0)=0$. It follows that

$$x_1(s) = \int_0^s \cos\theta\,\mathrm{d}s = \left(1 - \frac{2}{k^2}\right)s + \frac{4\lambda}{k^2}E\left(\frac{s}{2\lambda}\middle| k\right), \tag{22}$$

$$x_2(s) = \int_0^s \sin\theta\,\mathrm{d}s = \frac{4\lambda}{k^2}\left(\mathrm{dn}\left(\frac{s}{2\lambda}\middle| k\right) - 1\right), \tag{23}$$

where $E(s|k) = \int_0^s \mathrm{dn}^2(s|k)\,\mathrm{d}s$ is the incomplete elliptic integral of the second kind and we have removed two arbitrary constants by enforcing $x_1(0)=0$ and $x_2(0)=0$ [27]. Note that this solution possesses the symmetry $x_1(s) = -x_1(-s)$ and $x_2(s) = x_2(-s)$. The constants λ and k are determined by enforcing two constraints. For instance, we could specify the distance $x_1(L/4) - x_1(-L/4) = a$, as would be the case when a microtubule of length $a > L/\pi$ is placed inside the vesicle in such way that it pushes against the membrane. This leads to the equation

$$\left(1 - \frac{2}{k^2}\right)\frac{L}{4} + \frac{4\lambda}{k^2}E\left(\frac{L}{8\lambda}\middle| k\right) = \frac{a}{2}. \tag{24}$$

A second equation can be obtained by various means. One possibility is to impose

$$\theta\left(\frac{L}{4}\right) = 2\mathrm{am}\left(\frac{L}{8\lambda}\middle| k\right) = \theta_a, \tag{25}$$

where θ_a is an angle determined by the nature of the interaction between the membrane and the microtubule. A second possibility is to impose

$$\kappa\left(\frac{L}{4}\right) = \frac{1}{\lambda}\mathrm{dn}\left(\frac{L}{8\lambda}\middle| k\right) = 0, \tag{26}$$

which would be the case if the membrane exerts no moments on the microtubule at their point of intersection. Eqs. (24) and (25) or (26) are two equations in the two unknowns λ and k and can be solved numerically. The tension σ in the membrane is then easily determined from (21). The shape of the vesicle is obtained from (22) and (23) and is symmetric about the x_1- and x_2-axes. The results of this exercise are shown in Fig. 4 where the end-curvature, tension, bending energy and the vesicle shape are plotted as a function of the angle $\theta(L/4)$.

Note that the shapes seen in the experiment of Fygenson et al. [16] look ellipsoidal and similar to the shapes with $\theta(L/4) = 90^\circ$ (see Fig. 4) when the microtubule is only slightly longer than the diameter of the vesicle, while they have pronounced protrusions when the microtubules are much longer than the vesicle diameter. This suggests that there might be non-specific adhesive interactions between the microtubule and the vesicle when the microtubules are much longer than the diameter of the vesicle. Indeed, Fygenson et al. [28] mention that non-specific (adhesive) interactions between the tubulin monomers (that make up the microtubule) and the lipids (that make up the vesicle) are possible. When the microtubules are many times longer than the vesicle diameter cylindrical tethers are formed. Tether formation is imminent when the vesicle contour develops an inflection point close to the location where the microtubule impinges on it [16]. The angle made by the vesicle contour to the microtubule at this juncture can be determined by solving (24) and (25) and compared with the experiment. For instance, at $a/L = 0.37$, the angle $\theta(L/4) \approx 120^\circ$ when tubule formation is imminent

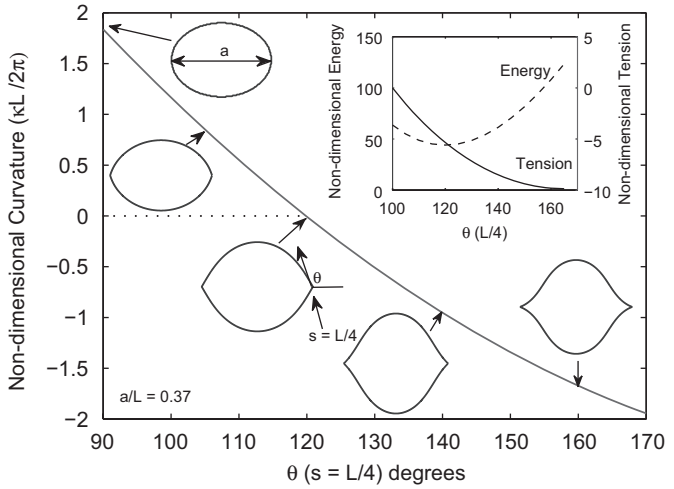

Fig. 4. The curvature is plotted as a function of the angle $\theta(L/4)$ made by the vesicle contour to the x_1-axis at $s = L/4$ for a particular ratio of the microtubule length a and vesicle contour length L. A larger magnitude of the end-curvature would imply a higher propensity for microtubule buckling. As the values of θ_a deviate from 90° the shapes have localized protrusions at the points where the microtubule interacts with the vesicle. This is similar to the observations of Fygenson et al. [16]. The inset shows the variation of the bending energy and the tension as a function of $\theta(L/4)$. The bending energy is a minimum at the angle where the curvature is zero. This would be the natural shape of the vesicle if the microtubule had no other interactions with the vesicle except impinging on it. Formation of vesicle shapes with pronounced protrusions suggests that there might be more complex interactions between the vesicle and microtubule.

(see Fig. 4) in our two-dimensional problem. If this angle (obtained by applying a zero curvature boundary condition in the axisymmetric case) is close to the one observed in the experiment then it would suggest that there are no adhesive/repulsive interactions between the microtubules and the vesicle. On the other hand, a large difference between the theoretical and experimental value of the angle θ_a would suggest that there are non-specific interactions between the microtubule and the lipids.

6. Conclusions

In this paper, we have obtained analytical solutions to the shape equations for a vesicle in two dimensions. Our solutions allow us to determine the vesicle shape under constraints of given length and given enclosed area. We used a numerical method to show that equilibrium multi-lobed vesicles are stable. Also, we have solved analytically for the shape of the vesicle when the distance between two points on the contour is constrained by the presence of a microtubule. We have shown that our two-dimensional theory is capable of producing shapes that are similar to those seen in the experiments of Fygenson et al. [16]. We believe that the results presented here provide valuable insight for the solution of the full axisymmetric shape equations. It is our future goal to solve the axisymmetric shape equations with the constraints imposed by the microtubule assuming no topology changes.

References

[1] M. Kraus, W. Wintz, U. Seifert, R. Lipowsky, Fluid vesicles in shear flow, Phys. Rev. Lett. 77 (1996) 3685–3688.
[2] U. Seifert, Configurations of fluid membranes and vesicles, Adv. Phys. 46 (1997) 13–137.
[3] E. Sackmann, Supported membranes: scientific and practical applications, Science 271 (1996) 43–48.
[4] T. Biben, K. Kassner, C. Misbah, Phase-field approach to three-dimensional vesicle dynamics, Phys. Rev. E 72 (2005).
[5] K.H. de Haas, C. Blom, D. van den Ende, M.H.G. Duits, J. Mellema, Deformation of giant lipid bilayer vesicles in shear flow, Phys. Rev. E 56 (1997) 7132–7137.
[6] C. Misbah, Vacillating breathing and tumbling of vesicles under shear flow, Phys. Rev. Lett. 96 (2006).
[7] V. Kantsler, V. Steinberg, Orientation and dynamics of a vesicle in tank-treading motion in shear flow, Phys. Rev. Lett. 95 (2005).
[8] V. Kantsler, V. Steinberg, Transition to tumbling and two regimes of tumbling motion of a vesicle in shear flow, Phys. Rev. Lett. 96 (2006).
[9] H. Noguchi, G. Gompper, Shape transitions of fluid vesicles and red blood cells in capillary flows, Proc. Natl. Acad. Sci. USA 102 (2005) 14159–14164.
[10] C. Pozrikidis, The axisymmetric deformation of a red blood cell in uniaxial straining Stokes flow, J. Fluid Mech. 216 (1990) 231–254.
[11] M.J. Stevens, Coarse-grained simulations of lipid bilayers, J. Chem. Phys. 121 (2004).
[12] Z. Ou-Yang, J. Liu, Y. Xie, Geometric Methods in the Elastic Theory of Membranes in Liquid Crystal Phases, World Scientific Publishing Co., 1999.
[13] G. Arreaga, R. Capovilla, C. Chryssomalakos, J. Guven, Area-constrained planar elastica, Phys. Rev. E 65 (2002).
[14] W. Shi, X. Feng, H. Gao, Two-dimensional model of vesicle adhesion on curved substrates, Acta Mech. Sinica 22 (2006) 529–535.
[15] U. Seifert, Adhesion of vesicles in two dimensions, Phys. Rev. A 43 (12) (1991) 6803–6814.
[16] D.K. Fygenson, J.F. Marko, A. Libchaber, Mechanics of microtubule-based membrane extension, Phys. Rev. Lett. 79 (1997) 4497.
[17] S.K. Veerapaneni, D. Gueyffier, D. Zorin, G. Biros, A boundary integral method for simulating the dynamics of inextensible vesicles suspended in a viscous fluid in 2d, Technical Report, University of Pennsylvania, 2008, To appear in the Journal of Computational Physics.
[18] V. Heinrich, B. Bozic, S. Svetina, B. Zeks, Vesicle deformation by an axial load: from elongated shapes to tethered vesicles, Biophys. J. 76 (1999) 2056–2071.
[19] V.A. Toponogov, Differential Geometry of Curves and Surfaces: A Concise Guide, A Birkhauser Book, 2006.
[20] H. Power, L. Wrobel, Boundary Integral Methods in Fluid Mechanics, Computational Mechanics Publications, 1995.
[21] A.G. Greenhill, The Applications of Elliptic Functions, Macmillan and Co., 1892.
[22] D. DeTurck, H. Gluck, D. Pomerleano, D.S. Vick, The four vertex theorem and its converse, Not. AMS 54 (2007).
[23] U.M. Ascher, L.R. Petzold, Computer Methods for Ordinary Differential Equations and Differential-Algebraic Equations, Society for Industrial and Applied Mathematics, Philadelphia, PA, USA, 1998.
[24] B.K. Alpert, Hybrid Gauss-trapezoidal quadrature rules, SIAM J. Sci. Comput. 20 (1999) 1551–1584.
[25] Y. Saad, Iterative Methods for Sparse Linear Systems, second ed., SIAM, Philadelphia, PA, 2003.
[26] M.A. Peterson, Deformation energy of vesicles at fixed volume and surface area, Phys. Rev. A 39 (1989) 2643–2645.
[27] A.E.H. Love, A Treatise on the Mathematical Theory of Elasticity, Dover, New York, 1944.
[28] D.K. Fygenson, M. Elbaum, B. Shraiman, A. Libchaber, Microtubules and vesicles under controlled tension, Phys. Rev. E 55 (1) (1997) 850–859.